Skin Layer of $BiFeO_3$ Single Crystals

Xavi Martí,[1,*] Pilar Ferrer,[2,3] Julia Herrero-Albillos,[4] Jackeline Narvaez,[5] Vaclav Holy,[1] Nick Barrett,[6] Marin Alexe,[7] and Gustau Catalan[5,8,†]

[1]*Charles University in Prague, Faculty of Mathematics and Physics, Czech Republic*
[2]*SpLine (BM25), ESRF, Grenoble, France*
[3]*Instituto de Ciencia de Materiales de Madrid ICMM-CSIC, Madrid, Spain*
[4]*Helmholtz-Zentrum Berlin für Materialien und Energie GmbH, Albert-Einstein-Straße 15, 12489 Berlin, Germany*
[5]*Centre d'Investigacions en Nanociencia i Nanotecnologia (CIN2), CSIC-ICN, Campus Bellaterra, 08193 Barcelona, Spain*
[6]*CEA, IRAMIS, SPCSI, LENSIS, F-91191 Gif-sur-Yvette, France*
[7]*Max Planck Institute of Microstructure Physics, Weinberg 2, 06120 Halle, Germany*
[8]*Institut Catala de Recerca i Estudis Avançats (ICREA), Catalunya, Spain*

(Received 6 December 2010; revised manuscript received 21 March 2011; published 6 June 2011)

A surface layer (''skin'') different from the bulk was found in single crystals of $BiFeO_3$. Impedance analysis and grazing incidence x-ray diffraction reveal a phase transition at $T^* \sim 275 \pm 5\,^{\circ}C$ that is confined within the surface of $BiFeO_3$. X-ray photoelectron spectroscopy and refraction-corrected x-ray diffraction as a function of incidence angle and photon wavelength indicate a reduced electron density and an elongated out-of-plane lattice parameter within a few nanometers of the surface. The skin will affect samples with large surface to volume ratios, as well as devices that rely on interfacial coupling such as exchange bias.

DOI: 10.1103/PhysRevLett.106.236101 PACS numbers: 68.35.B−, 61.05.cp, 68.35.Rh, 75.85.+t

Bismuth ferrite, $BiFeO_3$, has become a cornerstone of magnetoelectric research, owing to its high ferroelectric and magnetic ordering temperatures, large ferroelectric polarization, and electrically controllable magnetic easy plane [1–3]. Yet the phase diagram of this archetypal material still remains unresolved, with a growing number of structural and/or functional anomalies reported as a function of temperature that may or may not signal the existence of true phase transitions (see Ref. [3] for a critical review of some of them). Another unaddressed issue concerns the existence or otherwise of a surface layer (a ''skin'') in $BiFeO_3$. Notice that several important perovskites [e.g., $SrTiO_3$ [4,5], $BaTiO_3$ [6,7], or relaxor $Pb(Mg_{1/3}Nb_{2/3})O_3$ [8]] are known to have surface layers that are structurally different from the interior of the crystal. As we shall see, resolving the phase diagram of $BiFeO_3$ and unravelling its surface structure are in fact linked problems: the surface has its own symmetry and undergoes its own phase transitions which interfere with measurements of bulk $BiFeO_3$. Understanding the $BiFeO_3$ skin is also important because most devices proposed for this material rely on interfacial interactions such as exchange bias [2,9–11].

Here we have investigated the electronic and structural properties of the skin layer of $BiFeO_3$ single crystals as a function of temperature by techniques allowing a tunable information depth. We have found a phase transition at $T^* \sim 275 \pm 5\,^{\circ}C$ confined within the surface layer of the crystal. Meanwhile, at room temperature, refraction-corrected grazing incidence x-ray diffraction reveals that the skin of $BiFeO_3$ has an elongated out-of-plane lattice parameter (tensile strain of 0.7%) in the topmost few nanometers' region. Impedance spectroscopy and x-ray photoelectron spectroscopy show that the surface layer of $BiFeO_3$ is charge-depleted.

The crystal used for x-ray investigations was rosettelike with (001) habitus [12], grown using the method proposed by Kubel and Schmid [13]. It was first optically polished using sandpaper and diamond paste; subsequently, in order to minimize the mechanically damaged surface layer while preserving smoothness, a 30 min chemical-mechanical polishing using silica slurry (Syton SF1; Logitech) was employed. The pressure applied during the last stage was less than 100 g/cm^2 so as to minimize polishing stress at the surface. A photograph of the crystal is shown in Fig. 1 (inset). Ferroelectric or ferroelastic domains are optically observable using standard birefringence. The quadrant arrangement is consistent with the polarization pointing alternately along the diagonals of the unit cell, although closure cannot be confirmed by birrefringence alone. Precedents of ferroelectric flux closure have so far been limited to nanoscopic domains [14]. The local roughness was 0.8 nm, determined by atomic force microscopy, and in agreement with the x-ray reflectivity (Fig. 1) value of (1.3 ± 0.1) nm.

(110)-oriented dendritic crystals were also made as described in Refs. [15–18]. Their ac impedance [Figs. 2(a) and 2(b)] was measured using an Agilent impedance analyzer, model 4294A. The electrodes were sputtered gold, with Pt wires attached to them using silver paste. The impedance shows classic Maxwell-Wagner behavior [19]: a giant and frequency-dependent steplike increase in capacitance, typical of a material with two lossy dielectric

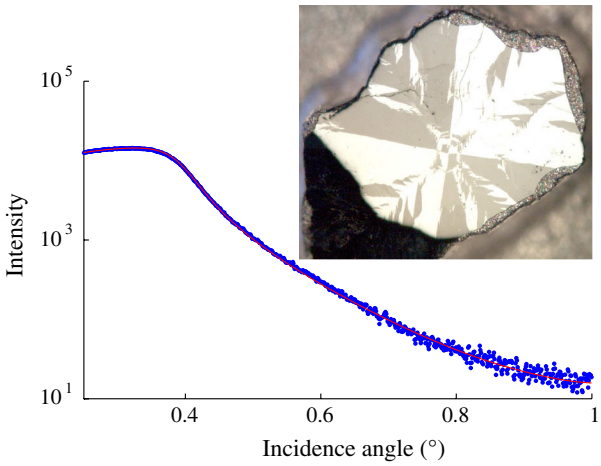

FIG. 1 (color online). X-ray reflectivity measurement (blue dots) and theoretical fit (solid red line) yielding a roughness of 1 nm for the surface of the $BiFeO_3$ crystal used in the diffraction study. Inset: Polarized optical microscopy view graph of the same mirror-polished single crystal, with habitus parallel to $\langle 001 \rangle_{\text{pseudocubic}}$, showing a quadrantlike arrangement of the four types of ferroelastic domain present in the sample.

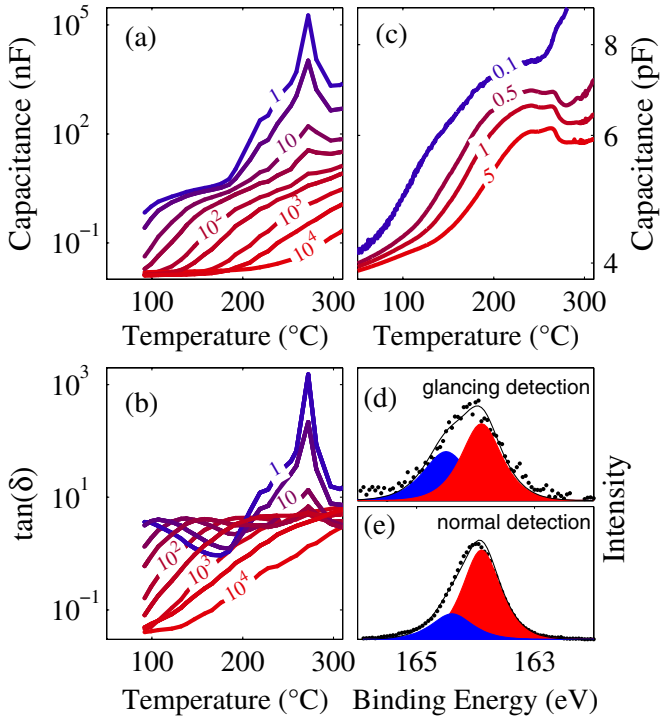

FIG. 2 (color online). Capacitive impedance measurements [panels (a), (b), and (c)]. The index in the curves indicates the frequency of the measurement in kHz. There is a peak at T ≅ 272 °C in the low-frequency region of the spectrum, which corresponds to the contact capacitance. This peak is absent at higher frequencies, so the transition does not affect the bulk. (c) The anomaly was also observed in unpolished crystals, so it is not caused by the polishing process. Panels (d) and (e): the XPS intensity at glancing detection (d) is shifted towards higher energies than that at normal incidence (e), consistent with a charge-depleted surface.

components in series. The bulk of the crystal becomes conducting as temperature increases (hence the large losses), so that the voltage is then mostly dropped on a charge-depleted interfacial barrier layer (contact capacitance); because the interface is thin, the *apparent* capacitance becomes large [20,21].

At low frequency (where interfacial capacitance dominates), there is a peak whose temperature ($T^* = 272\,^\circ\text{C}$) is frequency-independent thus signaling a true phase transition. On the other hand, the peak's absence from the high-frequency curves (where bulk capacitance dominates) implies that the inside of the crystal is not undergoing any change [22]. The T^* peak must therefore correspond to a phase transition confined within the interface. The anomaly is observed also in as-grown unpolished samples (Fig. 2(c)) and therefore the surface transition is not caused by polishing.

Further evidence for an electronically different surface layer comes from x-ray photoelectron spectroscopy (XPS). The Bi $4f$ core level results are shown in Figs. 2(d) and 2(e). Spectra were acquired at angles of 90° and 30° with respect to the sample surface using small spot Al $K\alpha$ radiation. Two components are observed in the Bi $4f$ spectrum indicating two different electronic environments for Bi^{3+}. The higher binding energy component is more intense at glancing angle detection [Fig. 2(d)] than at normal incidence [Fig. 2(e)], showing that it should be associated with the surface or near-surface region. No carbonate species were observed in the C $1s$ spectra (not shown); thus, the high binding energy component is not due to adsorbates. Higher binding energy is consistent with lower screening and therefore with lower electron density (charge depletion), as also observed in the skin of other ferroelectrics [6]. The Fe $2p$ spectrum was checked and showed a spin orbit splitting (13.45 eV) and $2p_{3/2}$ binding energy (710.8 eV), fully consistent with trivalent Fe. The XPS evidence thus points to a distinct electronic environment while maintaining the same chemistry as the bulk $BiFeO_3$.

Grazing incidence x-ray diffraction allows tracking surface structural changes, with tunable information depth from a few unit cells to several hundreds of microns [23]. The sample in Fig. 1 has been investigated by grazing incidence x-ray diffraction on the six-circle diffractometer at SpLine beam line, ESRF [25]. The sample was placed on a heating stage (25 °C–400 °C) covered with an airtight Kapton housing filled with 1 bar of pure oxygen to minimize oxygen vacancies.

In order to tune the penetration depth we have devised a dual approach, changing both the incidence angle and the incident photon energy. The justification is that, while either parameter alone permits probing different depths [Fig. 3(b); [23,24]], the parameters also yield refraction-induced peak shifts [26], so that both real (structural) shifts

and artificial (refractive) ones are convolved. In order to separate them we note that refraction behaves differently as a function of angle and energy [Fig. 3(b)], especially near the critical angle and/or the absorption edge (Bi L_3 at ~13 keV). The penetration depth δ and refractive shift ΔL plotted in Figs. 3(b) and 3(c) have been calculated using [23]

$$\delta = 1/\mathrm{Im}(q_z), \qquad \Delta L = a_z \mathrm{Re}(q_z - Q_z)/(2\pi),$$

where a_z is the vertical lattice parameter, and Q_z and q_z are the vertical components of the scattering vector in vacuum and in the material, respectively:

$$Q_z = K[\sin(\alpha_i) + \sin(\alpha_f)],$$

$$q_z = K[\sqrt{\sin^2(\alpha_i) - 2(1-n)} + \sqrt{\sin^2(\alpha_f) - 2(1-n)}],$$

with $\alpha_{i,f}$ the incidence and exit angles, n the complex refraction index, and $K = 2\pi/\lambda$ the wave vector length in vacuum. Figures 3(b) and 3(c) show that, at an incidence angle of 0.22°, the refraction shift is exactly the same for 10 keV and 15 keV. This set of angles and energies is therefore convenient because it allows discriminating penetration depths between a few angstroms and several tens of nanometers keeping a constant refraction.

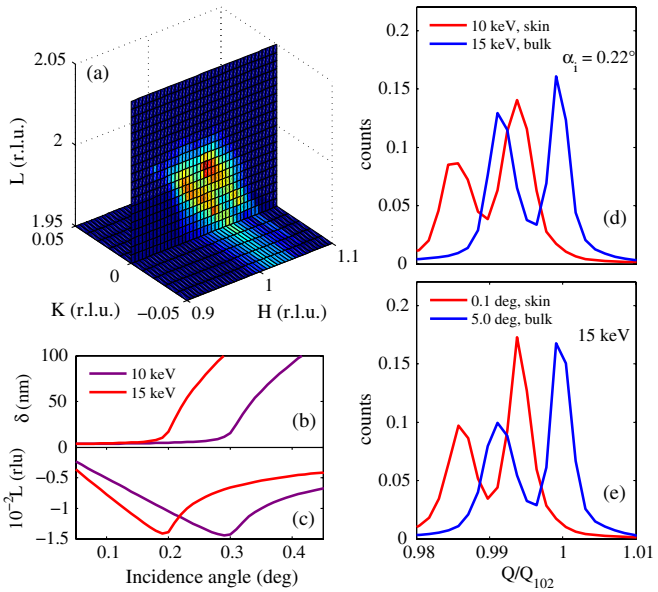

FIG. 3 (color online). (a) Reciprocal space tomograph around the (102) reflection. Calculated penetration depth (b) and refractive shift (c) as a function of incidence angle for two different beam energies, showing that for an angle of 0.22°, changing the energy allows tuning the penetration depth without changing the refractive shift. The Q-histogram analysis of the HKL measured by changing the photon energy (d) and the incidence angle (e), both of which confirm that the lattice parameter is expanded at the surface.

Diffracted intensity was mapped around the (102) reflection. We used a pseudocubic unit cell with perpendicular reciprocal lattice vectors H, K, and L, with L being perpendicular to the crystal surface. In Fig. 3(a) we show two perpendicular sections (tomographs) of the three-dimensional mesh. Because of the ferroelastic twinning, two peaks corresponding to the (102) and (− 102) reflections are observed. On top of this, there is broadening of the maxima due to mosaicity [27]. We have therefore tracked the *modulus* of the momentum transfer $Q = \sqrt{H^2 + K^2 + L^2}$, in analogy with powder diffraction, and used its changes to identify structural distortions.

Figures 3(d) and 3(e) show the radial distribution of intensities integrated for each shell of constant Q (i.e., the histogram of the moduli of Q) for the three-dimensional HKL maps. Fig. 3(d) shows data at identical incidence angle (0.22°) but different photon energies (10 and 15 keV); in 3(e) the photon energy is constant (15 keV) and the incidence angle is varied (0.1° and 5°). For each panel, the lighter (red) curve denotes the surface of the crystal, while the bulk is in the dark (blue) curve. We have normalized the intensities to allow a comparison between light (red) and dark (blue) curves, and corrected the peaks for refraction shift [26]. In all cases the data show an unambiguous difference between surface and bulk. Such a difference cannot be explained by refraction as the shift of the histograms was identical for all data in 3(d) and, moreover, the corrections in 3(e) lead to the same results. The conclusion is that there is an expansion of the (102) interplanar distance located at the topmost nanometers of the crystal. Since the skin must be in-plane coherent with the bulk, the peak shift translates into an out-of-plane lattice parameter elongation of 0.7% at the surface.

The temperature dependence of the out-of-plane lattice parameter has been measured and is shown in Fig. 4 for the bulk and for the surface ($\alpha_i = 0.1°$, penetration depth of 1 nm). The difference between the two curves is striking: whereas the bulk shows a featureless linear thermal expansion, the skin shows a marked anomaly, with negative thermal expansion setting in around 260 °C, followed by a sharp expansion of almost 0.2% at 280 °C. This temperature agrees with T^* from impedance analysis. Its detection only at the subcritical angle and absence from supercritical incidence confirms that the phase transition is confined within a skin layer that is only a few unit cells thick; though its exact thickness cannot be measured, the complete absence from x-ray measurements with a penetration depth of 50 nm places an upper bound and suggests an order of magnitude in the region of 10 nm or less.

Surface-sensitive probes such as backscattering Raman [28] have shown an onset of phonon softening at $T^* =$ 270 °C and culminating at T_N. It is not clear that it is the same transition, but the fact that T^* is the same is unlikely to be a coincidence. Skin effects may also account for other

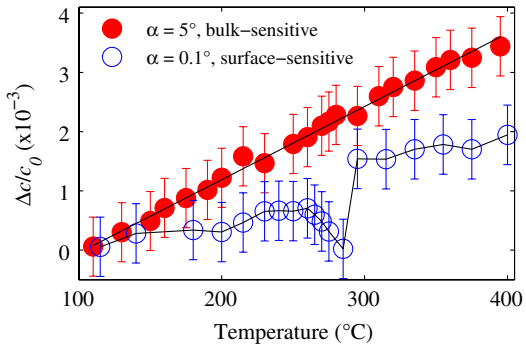

FIG. 4 (color online). Comparison between the reciprocal thermal expansion at the skin (empty symbols) and inside the crystal (solid symbols) evidencing the local phase transition at T^* in the surface of $BiFeO_3$.

unexplained anomalies of $BiFeO_3$ [3]. In particular, singularities at 200 K and 140 K have been observed by surface-sensitive probes [29,30] but not by bulk-sensitive ones such as transmission neutron diffraction and magnetometry [31], which suggests surface effects. As for the origin of the skin transition, the calculations of Dieguez *et al.* [32] predict a plethora of metastable phases within just 100 meV of the ground state of bulk $BiFeO_3$. A surface-confined transition would be facilitated by these, because the small energy barrier between them is of the same order as the surface relaxation energy of perovskites [33,34]. We also note that the (100) planes of $BiFeO_3$ are not neutral, so the electrostatic cost of the surface termination should also be considered, and may in fact contribute to the observed charge depletion.

The skin will impact on samples with a large surface to volume ratio. Fine grained ceramics, for example, are structurally different from large grained ones, with a melting of the Bi sublattice for a radius smaller than 9 nm [35], comparable to the thickness of the skin. Likewise, in thin films a T^* anomaly has been reported [36]. The distinct properties of the surface are also likely to affect the performance of interfacial coupling devices such as those based on exchange bias [11]. Given its repercussions, then, the surface of $BiFeO_3$ deserves close scrutiny from the multiferroic community.

We thank Professor Hans Schmid for the loan of one of the crystals used in this study, and for the critical reading of this manuscript. We also thank the SpLine staff for their assistance in using BM25B-SpLine and Pascale Jégou for the XPS measurements. We acknowledge financial support of the Spanish Ministerio de Ciencia e Innovación (PI201060E013), Consejo Superior de Investigaciones Científicas (PIE 200960I187), the German Science Foundation (Grant No. SFB762), Ministry of Education of Czech Republic (MSM0021620834), the Grant Agency of the Czech Republic (P204/11/P339), and of the EU (Project NAMASTE, 214499). M. A. and G. C. thank the Leverhulme trust for the funds that have enabled their collaboration.

*xavi.mr@gmail.com
†gustau.catalan@cin2.es

[1] W. Eerenstein *et al.*, Nature (London) **442**, 759 (2006).
[2] H. Bea *et al.*, J. Phys. Condens. Matter **20**, 434 221 (2008).
[3] G. Catalan and J. F. Scott, Adv. Mater. **21**, 2463 (2009).
[4] K. Hirota *et al.*, Phys. Rev. B **52**, 13195 (1995).
[5] S. Ravy *et al.*, Phys. Rev. Lett. **98**, 105501 (2007).
[6] X. L. Li *et al.*, Appl. Phys. Lett. **92**, 012902 (2008).
[7] I. A. Luk'yanchuk *et al.*, Phys. Rev. B **79**, 144111 (2009).
[8] G. Xu *et al.*, Phase Transit. **79**, 135 (2006).
[9] J. Dho *et al.*, Adv. Mater. **18**, 1445 (2006).
[10] D. Lebeugle *et al.*, Phys. Rev. Lett. **103**, 257601 (2009).
[11] S. M. Wu *et al.*, Nature Mater. **9**, 756 (2010).
[12] T. L. Burnett *et al.*, J. Cryst. Growth **285**, 156 (2005).
[13] F. Kubel and H. Schmid, J. Cryst. Growth **129**, 515 (1993).
[14] N. Balke *et al.*, Nature Nanotech. **4**, 868 (2009).
[15] C. Tabares-Muñoz, Ph.D. thesis, University of Geneva, Switzerland, 1986.
[16] C. Tabares-Muñoz *et al.*, Jpn. J. Appl. Phys. Pt. I **24**, 1051 (1985).
[17] R. Palai *et al.*, Phys. Rev. B **77**, 014110 (2008).
[18] D. Lebeugle *et al.*, Phys. Rev. Lett. **100**, 227602 (2008).
[19] A. Von Hippel, *Dielectrics and Waves* (John Wiley and Sons, New York, 1954).
[20] P. Lunkenheimer *et al.*, Phys. Rev. B **66**, 052105 (2002).
[21] G. Catalan and J. F. Scott, Nature (London) **448**, E4 (2007).
[22] J. F. Scott, JETP Lett. **49**, 233 (1989).
[23] U. Pietsch, V. Holy, and T. Baumbach, *High-Resolution X-ray Scattering: From Thin Films to Lateral Nanostructures* (Springer-Verlag, New York, 2004).
[24] B. Noheda *et al.*, Phys. Rev. Lett. **86**, 3891 (2001).
[25] G. R. Castro, J. Synchrotron Radiat. **5**, 657 (1998).
[26] M. F. Toney and S. Brennan, Phys. Rev. B **39**, 7963 (1989).
[27] From the angular broadening of the diffraction maxima we can estimate also the mean misorientation of the mosaic blocks: $\Delta\omega = (1.3 \pm 0.3)$ deg.
[28] R. Haumont *et al.*, Phys. Rev. B **73**, 132101 (2006).
[29] M. K. Singh *et al.*, J. Phys. Condens. Matter **20**, 252 203 (2008).
[30] M. Cazayous *et al.*, Phys. Rev. Lett. **101**, 037601 (2008).
[31] J. Herrero-Albillos *et al.*, J. Phys. Condens. Matter **22**, 256 001 (2010).
[32] Oswaldo Diéguez *et al.*, Phys. Rev. B **83**, 094105 (2011).
[33] J. Padilla and D. Vanderbilt, Phys. Rev. B **56**, 1625 (1997).
[34] J. Padilla and David Vanderbilt, Surf. Sci. **418**, 64 (1998).
[35] V. Petkov *et al.*, Phys. Rev. Lett. **105**, 185501 (2010).
[36] H. Toupet *et al.*, Phys. Rev. B **81**, 140101(R) (2010).